Mechanical Properties of Graphyne Monolayer: A First-Principles Study

Qing Peng [a], Wei Ji [b] and Suvranu De[b]

We investigated the mechanical properties of graphyne monolayer using first-principles calculations based on the Density Functional Theory. Graphyne has a relatively low in-plane Young's modulus (162 N/m) and a large Poisson ratio (0.429) compared to graphene. It can sustain large nonlinear elastic deformations up to an ultimate strain of 0.2 followed by a strain softening until failure. The single bond is more vulnerable to rupture than the triple bond and aromatic bond, although it has shorter bond length (0.19Å shorter) than aromatic bond. A rigorous continuum description of the elastic response is formulated by expanding the elastic strain energy density in a Taylor series in strain truncated after the fifth-order term. We obtained a total of fourteen nonzero independent elastic constants which are components of tensors up to tenth order. Pressure effect on the second-order elastic constants, in-plane Young's modules, and Poisson ratio are predicted. This study implies that graphyne-based surface acoustic wave sensors and waveguides may be synthesized by introducing precisely controlled local strains on graphyne monolayers.

1 INTRODUCTION

Presented in all known life forms, carbon provides the basis for life on Earth. Carbon has various hybridized states (sp, sp^2, and sp^3) and can form diverse bonding, with ability to bind to itself and to nearly all elements. As a consequence, carbon has numerous allotropes[1,2], such as graphene[3], fullerenes[4], carbon nanotubes[5], nanoringes[6], and nanobuds[7]. Synthesis and discovery of new carbon phases with high stability, novel bonding characteristics, unique properties and applications will be an ongoing effort for theoretical, synthetic and material scientists[2]. As new forms of non-natural carbon allotropes related to graphite/graphene, graphyne (Fig. 1) has been the subjects of interest due to their unique structures and intriguing electronic, optical and mechanical properties[8,9], and promising nanoelectronics and energy storage applications[10]. A very recent study indicates that graphyne is potentially superior to graphene in directional electrical conductivity[11].

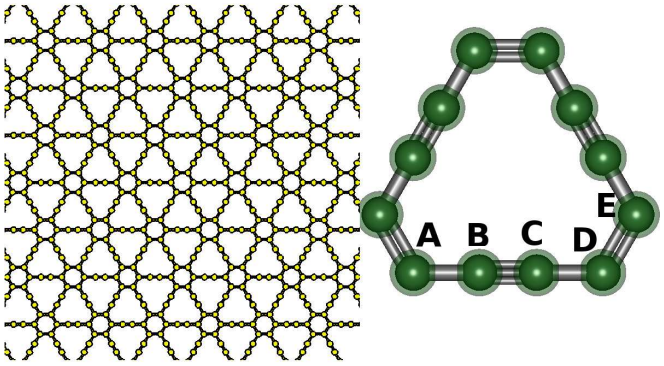

Fig. 1 Left: graphyne monolayer. Right: graphyne molecule.

Graphyne possess a remarkable planar network consisting of only benzene and alkyne units. The characteristic of this planar layered structure is the coexistence of sp^2 and sp hybridized carbon atoms, comprising aromatic benzene rings and weakly antiaromatic 12-membered rings[12,13]. Different from graphene/graphite, there are three types of C-C bonds in graphyne: C(sp^2)-C(sp^2) for the central aromatic ring (1.43 Å), C(sp^2)-C(sp) connecting the adjacent C=C and C≡C bonds (1.41 Å), and C(sp)-C(sp) for the linked triple bonds (1.22 Å). It has been pointed out that insertion of -C≡C- unit into each single bond of a molecule can form an expanded system and does not alter the molecule symmetry[14]. Graphyne monolayer has the same hexagonal symmetry ($p6m$) as graphene. Graphyne can be viewed as constructed from graphene by replacing one-third of the C-C bonds with C≡C linkages. It is predicted to have high temperature stability.

Graphyne was first proposed in 1987 by Baughman *et al.* [15]. Despite some attempts[16,17], the synthesis of graphyne has not yet been reported. Most recently, experimental success has been achieved in the synthesis of graphdiyne which is a substructure of graphyne[18,19]. Lacking experimental data, knowledge of the properties of this promising and interesting carbon allotrope depends on theoretical predictions. For electronic properties, Narita *et al.* reported the optimized lattice length (6.86 Å), binding energy (7.95 eV/atom), band gap (0.52 eV)[8]. Kondo *et al.* calculated the band gap of graphyne (0.89 eV) at the extended Huckel level[20]. Long *et al.* investigated the electronic structure and charge mobility of

[a] *Address: Department of Mechanical, Aerospace and Nuclear Engineering, Rensselaer Polytechnic Institute, Troy, NY 12180, U.S.A. Tel: 518-279-6669; E-mail: qpeng.org@gmail.com*

[b] *Address, Department of Mechanical, Aerospace and Nuclear Engineering, Rensselaer Polytechnic Institute, Troy, NY 12180, U.S.A.*

graphdiyne sheet and nanoribbons, which has a band gap of 0.46 eV.[21]. For compounds, Zhou *et al.* analyzed the nature of bonding and energy band structure of graphyne and its BN analog called "BN-yne"[22]. Their work showed that the band gap can be modulated by changing the size of hexagonal ring and the length of carbon chain. It is found that the high mobility of doped lithium and high energy storage capacity make graphyne a promising candidate for the anode material in battery applications[23]. Pan *et al.* explored the configurations and electronic properties of graphyne and graphdiyne nanoribbons with armchair and zigzag edges[24]. For mechanical properties, a classical molecular dynamics study has shown that unlike graphene, the fracture strain and stress of graphyne depend significantly on the direction of the applied strain and the alignment with carbon triple-bond linkages[25]. Kang *et al.* reported in-plane stiffness of graphyne monolayer as 166 N/m and Poisson's ratio 0.417[9].

There are some promising applications and recent development of the 2D materials, including high frequency field-effect transistors[26], graphene-based spintronics[27], ferromagnetics[28], antiferromagnetics[29], and nanoelectronics[30]. Due to monoatomic thickness, these 2D monolayers are very common to experience strain states during their applications, for example, mismatch strain and substrate surface corrugation[30,31]. Therefore, the knowledge of mechanical properties of graphyne is highly desired. Several previous studies have shown that 2D monolayers present a large nonlinear elastic deformation during the tensile strain up to the ultimate strength of the material followed by a strain softening until fracture[32–35]. We expect that the graphyne behaves in a similar manner.

Under large deformation, the strain energy density need to be expanded in a Taylor series to include quadratic and higher order terms in strain. The higher order terms account for both nonlinearity and strain softening of the elastic deformation. They can also express other anharmonic properties of 2D nanostructures including phenomena such as thermal expansion, phonon-phonon interaction, etc[36]. Despite the importance, the high order non-linear elastic properties of the 2D graphyne are still unknown.

The goal of this paper is to study the mechanical behaviors at large strains and find an accurate continuum description of the elastic properties of graphyne from *ab initio* density functional theory calculations. The total energies of the system, forces on each atoms, and stresses on the simulation boxes are directly obtained from DFT calculations. The response of graphyne under the nonlinear deformation and fracture are studied, including ultimate strength and ultimate strain. The high order elastic constants are obtained by fitting the stress-strain curves to analytical stress-strain relationships that belong to the continuum formulation[33]. Our results of continuum formulation could also be useful in finite element modeling of the multiscale calculations mechanical properties of graphyne in continuum level. The remainder of the paper is organized as follows. Section 2 presents the basic nonlinear elastic theory applied to 2D hexagonal structures. The computational details of DFT calculations are in section 3. The results and analysis are in section 4, followed by conclusions in section 5.

2 NONLINEAR ELASTICITY THEORY

We consider a primitive unit cell containing 12 atoms in one plane, with periodic boundary conditions. The undeformed reference configuration is shown in Fig. 2, with lattice vectors $\mathbf{H_i}$, $i = 1,2,3$. When a macroscopically homogeneous deformation with gradient tensor $\mathbf{F}$[37] is applied, the lattice vectors of the deformed graphyne are $\mathbf{h}_i = \mathbf{F}\mathbf{H}_i$. The Lagrangian strain[38] is defined as $\boldsymbol{\eta} = \frac{1}{2}(\mathbf{F}^T\mathbf{F} - \mathbf{I})$, where $\mathbf{I}$ is the identity tensor. For a hyperelastic materials, the strain energy density has functional form of $\Phi = \Phi(\eta)$ and the components of the symmetric second Piola-Kirchhoff stress tensor (Σ) can be expressed as

$$\Sigma_{ij} = \frac{\partial \Phi}{\partial \eta_{ij}}. \tag{1}$$

Using Taylor's series expansion up to fifth order, the above relationship may be written as

$$\begin{aligned}\Sigma_{ij} =& C_{ijkl}\eta_{kl} + \frac{1}{2!}C_{ijklmn}\eta_{kl}\eta_{mn} + \frac{1}{3!}C_{ijklmnop}\eta_{kl}\eta_{mn}\eta_{op} \\ &+ \frac{1}{4!}C_{ijklmnopqr}\eta_{kl}\eta_{mn}\eta_{op}\eta_{qr}.\end{aligned} \tag{2}$$

Einstein's summation convention has been employed for repeating indices which range from 1 to 3. Herein $\mathbf{C}$ denotes each higher-order elastic modulus tensor; the rank of each tensor corresponds to the number of subscripts. The second-order elastic constants (SOEC) C_{ijkl}, third-order elastic constants (TOEC), C_{ijklmn}, fourth-order elastic constants (FOEC), $C_{ijklmnop}$, and fifth- order elastic constants (FFOEC), $C_{ijklmnopqr}$, are given by the components of the fourth-, sixth-, eighth-, and tenth-rank tensors, respectively.

Using conventional Voigt notation[39] for subscripts: $11 \rightarrow 1$, $22 \rightarrow 2$, $33 \rightarrow 3$, $23 \rightarrow 4$, $31 \rightarrow 5$, and $12 \rightarrow 6$. Please note that for strain $\eta_4 = 2\eta_{23}$, $\eta_5 = 2\eta_{31}$, $\eta_6 = 2\eta_{12}$. Eqn. 2 can be rewritten as

$$\begin{aligned}\Sigma_I =& C_{IJ}\eta_J + \frac{1}{2!}C_{IJK}\eta_J\eta_K + \frac{1}{3!}C_{IJKL}\eta_J\eta_K\eta_L \\ &+ \frac{1}{4!}C_{IJKLM}\eta_J\eta_K\eta_L\eta_M.\end{aligned} \tag{3}$$

where the upper case indices are from 1 to 6.

We modeled the monolayer graphyne as a two-dimensional (2D) structure and assume that the deformed state of the

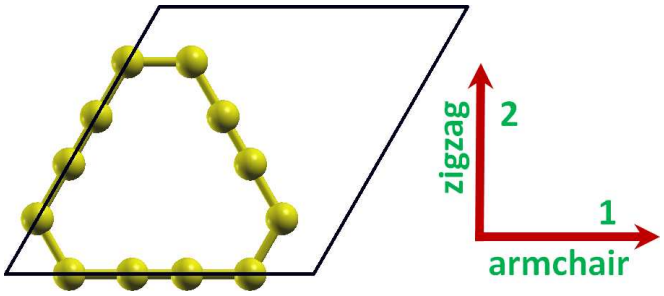

Fig. 2 Atomic structure of graphyne monolayer in the primitive unit cell (12 atoms) in the undeformed reference configuration.

monolayer graphyne is such that the contribution of bending to the strain energy density is negligible, compared to the in-plane strain contribution. This assumption is reasonable since the radius of curvature of out-of-plane deformation is significantly larger than the in-plane inter-atomic distance. The stress state of monolayer graphyne under those assumptions can be assumed to be 2D and we only consider the in-plane stress and strain components for these kind of structures.

For a general deformation state the number of independent components of the second, third, fourth and fifth order elastic tensors is 21, 56, 126, and 252, respectively. However, there are only fourteen independent elastic constants need to be explicitly considered due to the symmetries of the atomic lattice point group D_{6h} which consists of a six-fold rotational axis and six mirror planes[35].

The fourteen independent elastic constants of graphyne are determined by a least-squares fit to stress-strain results from DFT based first-principles studies in two steps, detailed in our previous work[34]. In the first step, we use a least-squares fit to five stress-strain responses. Five relationships between stress and strain are necessary because there are five independent FFOECs. We obtain the stress-strain relationships by simulating the following deformation states: uniaxial strain in the zigzag direction; uniaxial strain in the armchair direction; and biaxial strain. From the first step, the components of SOEC, TOEC, FOEC are over-determined (i.e, the number of linearly independent variables are greater than the number of constrains), and the FFOEC are well-determined (the number of linearly independent variables are equal to the number of constrains). Under such circumstance, the second step is needed: least-square solution to these over- and well- determined linear equations.

3 DENSITY FUNCTIONAL THEORY CALCULATIONS

The stress-strain relationship of graphyne under the desired deformation configurations is characterized via first-principles calculations with the density-functional theory (DFT). DFT calculations were carried out with the Vienna Ab-initio Simulation Package (VASP)[40–43] which is based on the Kohn-Sham Density Functional Theory (KS-DFT)[44,45] with the generalized gradient approximations as parameterized by Perdew, Burke and Ernzerhof (PBE) for exchange-correlation functions[46]. The electrons explicitly included in the calculations are the ($2s^2 2p^2$) electrons. The core electrons ($1s^2$) are replaced by the projector augmented wave (PAW) and pseudopotential approach[47,48]. A plane-wave cutoff of 400 eV is used in all the calculations. The calculations are performed at zero temperature.

The criterion to stop the relaxation of the electronic degrees of freedom is set by total energy change to be smaller than 0.000001 eV. The optimized atomic geometry was achieved through minimizing Hellmann-Feynman forces acting on each atom until the maximum forces on the ions were smaller than 0.01 eV/Å.

The atomic structures of all the deformed and undeformed configurations are obtained by fully relaxing a 12-atom-unit cell where all atoms were placed in one plane. The simulation invokes periodic boundary conditions for the two in-plane directions while the displacement to out-of-plane direction is forbidden.

The irreducible Brillouin Zone was sampled with a Gamma-centered $11 \times 11 \times 1$ k-mesh. Such large k-mesh was used to reduce the numerical errors caused by the strain of the systems. The initial charge densities were taken as a superposition of atomic charge densities. There was a 11 Å thick vacuum region to reduce the inter-layer interaction to model the single layer system. The results of the calculations are independent of the precise value of the out-of-plane thickness, so there is no physical interpretation attached to the quantity.

The VASP simulation calculates the true or Cauchy stresses, σ, which for monolayer graphyne must be expressed as a 2D force per length with units of N/m by taking the product of the Cauchy stresses (with units of N/m^2) and the super-cell thickness of 11 Å. The Cauchy stresses are related to the second Piola-Kirchhoff (PK2) stresses $\mathbf{\Sigma}$ as

$$\mathbf{\Sigma} = J\mathbf{F}^{-1}\sigma(\mathbf{F}^{-1})^T \tag{4}$$

where J=det($\mathbf{F}$).

4 RESULTS AND ANALYSIS

4.1 Atomic Structure

We first optimize the equilibrium lattice constant for monolayer graphyne. The total energy as a function of lattice spacing is obtained by specifying nine lattice constants varying from 6.5 Å to 7.3 Å, with full relaxations of all the atoms. A least-square fit of the energy vs. lattice constant with a

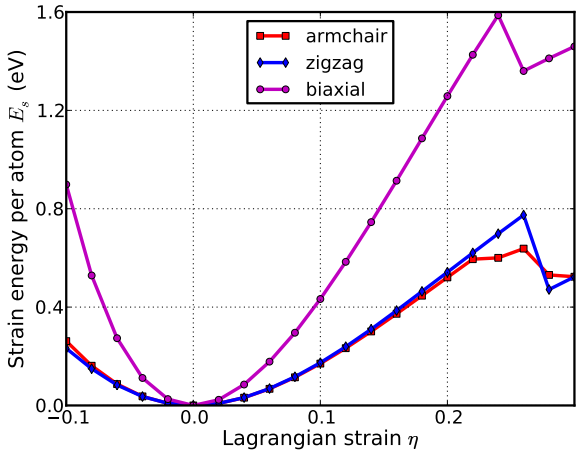

Fig. 3 Energy-strain responses for uniaxial strain in armchair and zigzag directions, and biaxial strains.

fourth-order polynomial function yields the equilibrium lattice constant as 6.889 Å. The result is in good agreement with previous DFT calculations[9,22].

The most energetically favorable structure is set as the strain-free structure in this study and the atomic structure, as well as the primitive cell is shown in Fig. 2. Specifically, the bond length of the triple bond between atom B and C (marked in Fig. 1) is 1.223 Å. The largest bond length is the aromatic bond between atom D and atom E, which is 1.426 Å, slightly longer than that of a pristine graphene sheet (1.425 Å) due to the presence of the acetylene groups. The single bond between atom A and B (symmetrically C and D) is 1.407 Å, shorter than the typical value of 1.47 Å. The contraction of the single bonds is due to the charge transfer from the benzene ring to the acetylene group[22].

4.2 Strain Energy

When the strains are applied, all the atoms are allowed full freedom of motion within their plane. A quasi-Newton algorithm is used to relax all atoms into equilibrium positions within the deformed unit cell that yields the minimum total energy for the imposed strain state of the super cell.

Both compression and tension are considered with Lagrangian strains ranging from -0.1 to 0.3 with an increment of 0.02 in each step for all three cases. We define strain energy per atom $E_s = (E_{tot} - E_0)/n$, where E_{tot} is the total energy of the strained system, E_0 is the total energy of the strain-free system, and $n = 12$ is the number of atoms in the unit cell. Fig. 3 shows the E_s as a function of strain in uniaxial armchair, uniaxial zigzag and biaxial deformation. E_s is seen to be anisotropic with strain direction. E_s is non-symmetrical for compression ($\eta < 0$) and tension ($\eta > 0$) for all three cases. This non-symmetry indicates the anharmonicity of the monolayer graphyne structures.

4.3 Stress-strain Relationships

The second P-K stress versus Lagrangian strain relationship for uniaxial strains along the armchair and zigzag directions and biaxial strains are shown in Fig. 4. The ultimate strength is the maximum stress that a material can withstand while being stretched, and the corresponding strain is the *ultimate* strain.

In general, the drop of the strain energy in the energy-strain curve indicates the internal structure changes. The corresponding strain of the maximum strain energy is the *critical* strain. The stresses are the derivatives of the strain energies with respect to the strains. Under ideal conditions, the critical strain is larger than the ultimate strain. The systems of perfect graphyne under strains beyond the ultimate strains are in a metastable state, which can be easily destroyed by long wavelength perturbations, vacancy defects, as well as high temperature effects[49]. The ultimate strain is determined by the intrinsic bonding strengths and acts as a lower limit of the fraction strain. Thus it has practical meaning in considering for its applications.

The ultimate strengths and strains corresponding to the different strain conditions in Fig. 4 are in Table 1, compared with those of graphene and previous molecular dynamics study[25]. Graphyne has much lower ultimate strengths, about 2/3 of these of graphene. It also has smaller ultimate strains under the zigzag and biaxial strains. However, it has larger ultimate strain under the armchair strain. This could be due to the release of the pre-contracted single C-C bonds parallel to the armchair direction. Our results of ultimate stress and strain are quite different form the predictions of previous molecular dynamics study[25]. This might indicate that the DFT method is more suitable in studying this 2D material under extreme conditions of large strain and stresses ($>$ 50 GPa) than a force field method.

The material behaves in an asymmetric manner with respect to compressive and tensile strains. With increasing strains, the bonds are stretched and eventually rupture. The insets in Fig. 4 shows the atomic structure of graphyne at ultimate strain. When strained in the armchair direction, once the bond lengths of single bonds along the armchair direction are elongated more than 1.08 times its value at zero strain, the bonds are considered to be ruptured (Fig. 4a). However, it is the aromatic bond between atoms D and E that ruptures when the structure is loaded in the zigzag direction (Fig. 4b). All the single bonds rupture when loaded in the biaxial direction (Fig. 4c). Our results show that the single bond is more vulnerable to rupture than the triple bond and aromatic bond, although it has shorter bond length (0.19Å shorter) than aro-

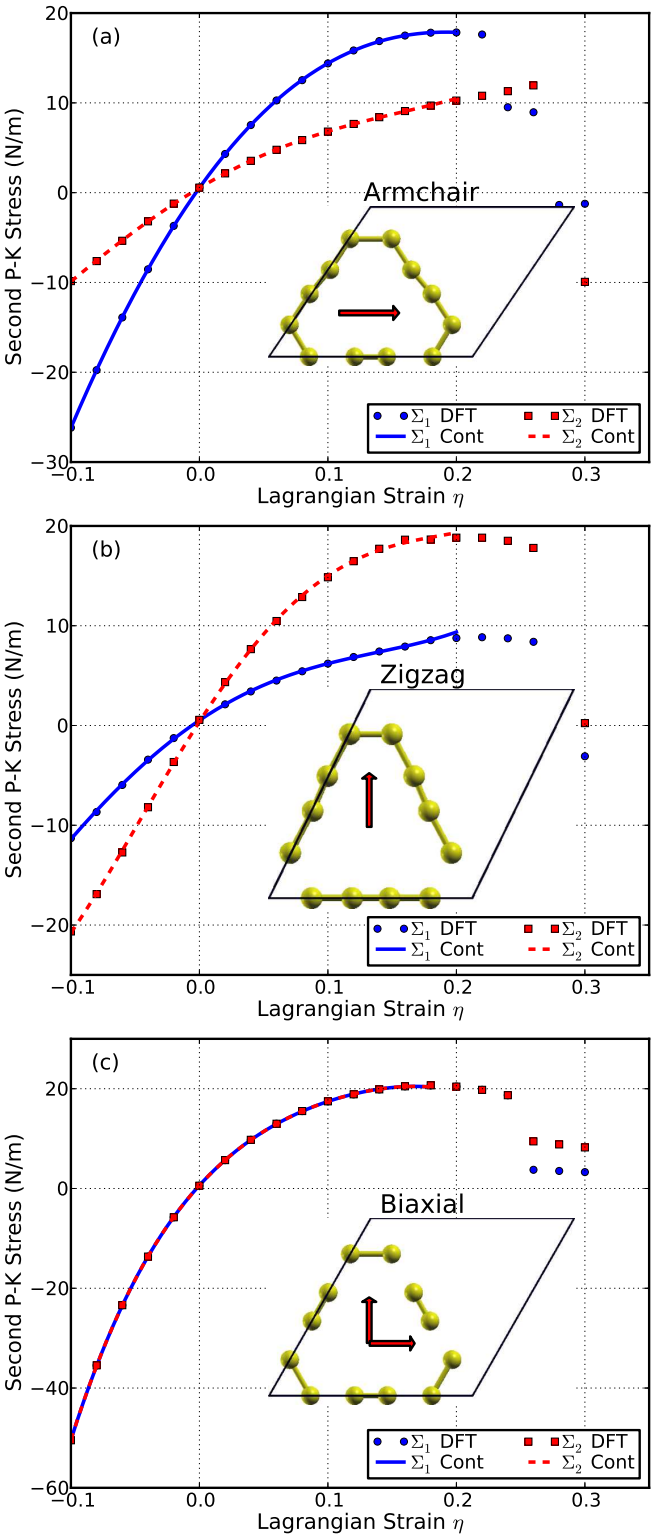

Fig. 4 Stress-strain response for (a) uniaxial strain along the armchair direction, (b) uniaxial strain along the zigzag direction and (c) biaxial strain. Σ_1 (Σ_2) denotes the x (y) component of stress. "Cont" stands for the fitting of DFT calculations ("DFT") to continuum elastic theory.

Table 1 Ultimate strengths (Σ_m^a,Σ_m^z,Σ_m^b) in units of N/m and ultimate strains (η_m^a, η_m^z, η_m^b) under uniaxial strain (armchair and zigzag) and biaxial of graphyne from DFT calculations, compared with graphene and previous molecular dynamics (MD) study.

	Graphyne	Graphyne(MD)[25]	Graphene[50]
Σ_m^a	17.84	14.34†	28.56
η_m^a	0.2	0.08	0.18
Σ_m^z	18.83	31.97†	30.36
η_m^z	0.2	0.12	0.22
Σ_m^b	20.64	-	32.01
η_m^b	0.18	-	0.22

† The value is converted from original data (in units of GPa) obtained with "Energy minimization" using the 3.20 Å in thickness assumed in ref[25].

matic bond.

4.4 Elastic Constants

The elastic constants are critical parameters in finite element analysis models for mechanical properties of materials. Our results of these elastic constants provide an accurate continuum description of the elastic properties of graphyne from ab initio density functional theory calculations. They are suitable for incorporation into numerical methods such as the finite element technique.

The second elastic constants model the linear elastic response. The higher (> 2) order elastic constants are important to characterize the nonlinear elastic response of graphyne using a continuum description. These can be obtained using a least squares fit of the DFT data and are reported in Table 2. Corresponding values for graphene are also shown.

The in-plane Young's modulus Y_s and Poison's ratio ν may be obtained from the following relationships: $Y_s = (C_{11}^2 - C_{12}^2)/C_{11}$ and $\nu = C_{12}/C_{11}$. Our results of $Y_s = 162.1$ (N/m) and $\nu = 0.429$ are comparable with previous *ab initio* prediction ($Y_s = 166$ (N/m) and $\nu = 0.417$)[9]. The in-plane Young's modulus of graphyne is quite small (47%) compared to graphene, which indicates that the graphyne is very soft. The small in-plane Young's modulus could be understood as by two facts. First the average coordination number of an atom in graphyne is 2.5, less than those in graphene, which are 3.0. As a consequence, the number of bonds in graphyne is fewer than that of graphene. Second, the in-plane atomic mass density and the electronic charge density of graphyne are smaller (0.77 times) than those of graphene.

However, graphyne has a Poisson's ratio which is twice as large as graphene. Recall that a perfectly incompressible material has a Poisson's ratio of 0.5. Hence, graphyne is observed to conserve volume well under uniaxial strains.

Table 2 Nonzero independent components for the SOEC, TOEC, FOEC and FFOEC tensor components (in units of N/m), Poisson's ration ν and in-plane Young's modulus Y_s of graphyne from DFT calculations, compared with graphene.

	Graphyne	Graphene[50]	Graphene[35]
a	6.889	2.468	2.446
Y_s	162.1	344.6	348
ν	0.429	0.179	0.169
C_{11}	198.7	356.0	358.1
C_{12}	85.3	63.7	60.4
C_{111}	-890.9	-3120.9	-2817
C_{112}	-872.6	-471.7	-337.1
C_{222}	-1264.2	-2978.1	-2693.3
C_{1111}	-7966	19980	13416.2
C_{1112}	4395	2706	759
C_{1122}	8662	2843	2582.8
C_{2222}	1154	16568	10358.9
C_{11111}	89000	-81498	-31383.8
C_{11112}	-10393	-13378	-88.4
C_{11122}	-26725	-12852	-12960.5
C_{12222}	15495	-28504	-13046.6
C_{22222}	14262	-79311	-33446.7

The knowledge of higher order elastic constants is very useful to understand the anharmonicity. Especially, third-order elastic constants are important in understanding the nonlinear elasticity of materials such as changes in acoustic velocities due to finite-strain. With third-order elastic moduli, we can study the effect of the second-order elastic moduli on the pressure p acting in the plane of graphyne monolayer. Explicitly, when pressure is applied, the pressure dependent second-order elastic moduli ($\tilde{C_{11}}$, $\tilde{C_{12}}$, $\tilde{C_{22}}$) can be obtained from C_{11}, C_{12}, C_{22}, C_{111}, C_{112}, C_{222}, Y_s, ν, as formulated in Ref[34].

The second-order elastic moduli of graphyne are seen to increase linearly with the applied pressure (Fig. 5). Poisson's ratio also increases monotonically with the increase of pressure. $\tilde{C_{11}}$ is not symmetrical to $\tilde{C_{22}}$ any more. Only when $P = 0$, $\tilde{C_{11}} = \tilde{C_{22}} = C_{11}$. This anisotropy could be the outcome of anharmonicity.

Graphyne monolayers exhibit instability under large tension. All stress-strain curves in the previous section show that graphyne will soften when the strain is larger than the ultimate strain. From the view of electron bonding, this is due to the bond weakening and breaking. This softening behavior is determined by the TOECs and FFOECs in continuum aspect. The negative values of TOECs and FFOECs ensure the softening of graphyne monolayer under large strain.

The hydrostatic terms (C_{11}, C_{22}, C_{111}, C_{222}, and so on) of graphyne monolayers are smaller than those of graphene, consistent with the conclusion that the graphyne is "softer". The shear terms (C_{12}, C_{112}, C_{1122} etc.) in general are larger than those of graphene, which contributes to its less compressibility.

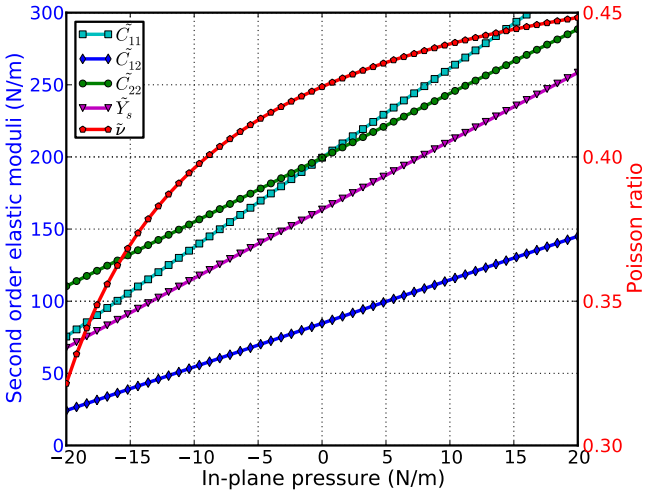

Fig. 5 Second-order elastic moduli and Poisson ratio as function of the pressure.

4.5 Promising Applications

In graphyne monolayer, there are non-zero in-plane Young's modulus and shear deformations. Hence, it is possible to generate sound waves with different velocities depending on the deformation mode. Sound waves generating biaxial deformations (compressions) are compressional or p-waves. Sound waves generating shear deformations are shear or s-waves. The sound velocities of these two types of waves are calculated from the second-order elastic moduli and mass density using the following relations:

$$v_p = \sqrt{\frac{\tilde{Y_s}(1-\tilde{\nu})}{\rho_m(1+\tilde{\nu})(1-2\tilde{\nu})}}, \tag{5}$$

$$v_s = \sqrt{\frac{\tilde{C_{12}}}{\rho_m}}. \tag{6}$$

The dependence of v_p and v_s on pressure (biaxial stress) is plotted in Fig. 6. Both v_p and v_s monotonically increase with increase in pressure. Thus they can be tuned by introducing the biaxial strain through the stress-strain relationship shown in Fig. 4c.

Compressional to shear wave velocity ratio (v_p/v_s) is a very useful parameter in the determination of the materials mechan-

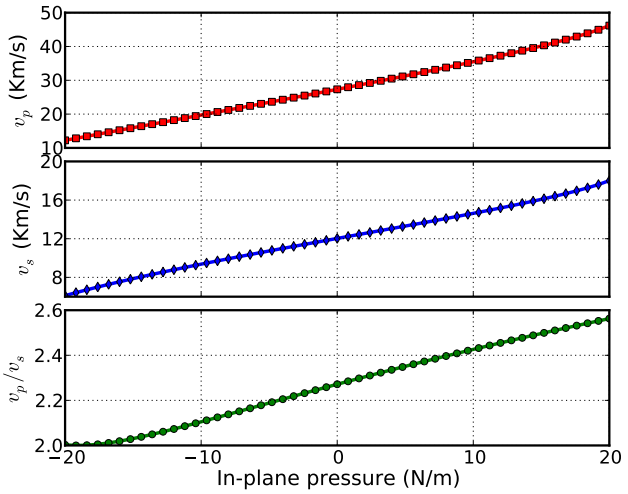

Fig. 6 *p*-wave and *s*-wave velocities, and compressional to shear wave velocity ratio v_p/v_s as a function of in-plane pressure.

ical properties. It depends only on the Poisson's ratio as

$$\frac{v_p}{v_s} = \sqrt{\frac{1}{\tilde{\nu}}(1+\frac{\tilde{\nu}^2}{1-2\tilde{\nu}})}. \quad (7)$$

The ratio of v_p/v_s monotonically increases with the increase of pressure as shown in Fig. 6.

Notice that a sound velocity gradient could be achieved by introducing stress into a graphyne monolayer, which could lead to refraction of sound wavefronts in the direction of lower sound speed, causing the sound rays to follow a curved path[51]. The radius of curvature of the sound path is inversely proportional to the gradient. Also a negative sound speed gradient could be achieved by a negative strain gradient. This tunable sound velocity gradient can be used to form a sound frequency and ranging channel, which is the functional mechanism of waveguides and surface acoustic wave (SAW) sensors[52,53]. Thus, graphyne-based nano-devices of SAW sensors, filters and waveguides may be synthesized using local strains for next generation electronics.

5 CONCLUSIONS

We studied the mechanical response of graphyne monolayer under various strains using DFT based first-principles calculations. The bond lengths of the single, triple, and aromatic bonds are 1.407 Å , 1.223 Å , and 1.426 Å , respectively. The single bond is more vulnerable to rupture than the triple bond and aromatic bond, although it has shorter bond length than aromatic bond. Graphyne monolayers exhibit a nonlinear elastic deformation up to an ultimate strain of 0.2, followed by a strain softening until failure. The deformation and failure behavior and the ultimate strength are anisotropic. The ultimate strength in biaxial strain is about 2.81 N/m and 1.81 N/m larger than that in the armchair and zigzag directions, respectively.

We found an accurate continuum description of the elastic properties of graphyne by explicitly determining the fourteen independent components of high order (up to fifth order) elastic constants from the fitting of the stress-strain curves obtained from DFT calculations. This data is useful to develop a continuum description which is suitable for incorporation into a finite element analysis model for its applications in large scale.

Pressure effect on the second-order elastic constants, in-plane Young's modules, and Poisson ratio are predicted. Graphyne is observed to have a relatively low in-plane Young's modulus (162 N/m) and a large Poisson ratio (0.429) compared to graphene. Another interesting observation is that local variations of pressure, introduced by external stresses could be used to modulate the velocity of sound waves in graphyne. Hence, graphyne-based nanodevices or SAW sensors and waveguides could be synthesized by introducing local strain for next generation electronic devices.

ACKNOWLEDGEMENTS

We thank Dr. Zhongfang Chen for helpful discussions. The authors would like to acknowledge the generous financial support from the Defense Threat Reduction Agency (DTRA) Grant # BRBAA08-C-2-0130, the U.S. Nuclear Regulatory Commission Faculty Development Program under contract # NRC-38-08-950, and U.S. Department of Energy (DOE) Nuclear Energy University Program (NEUP) Grant # DE-NE0000325.

References

1 F. Diederich and M. Kivala, *Adv. Mater.*, 2010, **22**, 803.
2 A. Hirsch, *Nature Mater.*, 2010, **9**, 868.
3 K. S. Novoselov, A. K. Geim, S. V. Morozov, D. Jiang, Y. Zhang, S. V. Dubonos, I. V. Grigorieva and A. A. Firsov, *Science*, 2004, **306**, 666.
4 H. W. Kroto, J. R. Heath, S. C. Obrien, R. F. Curl and R. E. Smalley, *Nature*, 1985, **318**, 162.
5 S. Iijima, *Nature*, 1991, **354**, 56.
6 X. Y. Kong, Y. Ding, R. Yang and Z. L. Wang, *Science*, 2004, **303**, 1348.
7 A. G. Nasibulin, P. V. Pikhitsa, H. Jiang, D. P. Brown, A. V. Krasheninnikov, A. S. Anisimov, P. Queipo, A. Moisala, D. Gonzalez, G. Lientschnig, A. Hassanien, S. D. Shandakov, G. Lolli, D. E. Resasco, M. Choi, D. Tomanek and E. I. Kauppinen, *Nature Nanotech*, 2007, **2**, 156.

8 N. Narita, S. Nagai, S. Suzuki and K. Nakao, *Phys. Rev. B*, 1998, **58**, 11009.

9 J. Kang, J. Li, F. Wu, S.-S. Li and J.-B. Xia, *J. Phys. Chem. C*, 2011, **115**, 20466.

10 K. Srinivasu and S. K. Ghosh, *J. Phys. Chem. C*, 2012, **116**, 5951–5956.

11 D. Malko, C. Neiss, F. Vines and A. Goerling, *Phys. Rev. Lett.*, 2012, **108**, 086804.

12 K. Tahara, T. Yoshimura, M. Sonoda, Y. Tobe and R. V. Williams, *The Journal of Organic Chemistry*, 2007, **72**, 1437–1442.

13 J. Juselius and D. Sundholm, *Phys. Chem. Chem. Phys.*, 2001, **3**, 2433–2437.

14 R. Chauvin, *Tetrahedron Letters*, 1995, **36**, 397.

15 R. H. Baughman, H. Eckhardt and M. Kertesz, *J. Chem. Phys.*, 1987, **87**, 6687.

16 J. M. Kehoe, J. H. Kiley, J. J. English, C. A. Johnson, R. C. Petersen and M. M. Haley, *Organic Lett.*, 2000, **2**, 969.

17 T. Yoshimura, A. Inaba, M. Sonoda, K. Tahara, Y. Tobe and R. V. Williams, *Organic Lett.*, 2006, **8**, 2933.

18 G. Li, Y. Li, H. Liu, Y. Guo, Y. Li and D. Zhu, *Chem. Communc.*, 2010, **46**, 3256.

19 G. Li, Y. Li, X. Qian, H. Liu, H. Lin, N. Chen and Y. Li, *J. Phys. Chem. C*, 2011, **115**, 2611.

20 M. Kondo, D. Nozaki, M. Tachibana, T. Yumura and K. Yoshizawa, *Chem. Phys.*, 2005, **312**, 289.

21 M. Long, L. Tang, D. Wang, Y. Li and Z. Shuai, *ACS NANO*, 2011, **5**, 2593.

22 J. Zhou, K. Lv, Q. Wang, X. S. Chen, Q. Sun and P. Jena, *J. Chem. Phys.*, 2011, **134**, 174701.

23 H. Zhang, M. Zhao, X. He, Z. Wang, X. Zhang and X. Liu, *J. Phys. Chem. C*, 2011, **115**, 8845.

24 L. D. Pan, L. Z. Zhang, B. Q. Song, S. X. Du and H. J. Gao, *Appl. Phys. Lett.*, 2011, **98**, 173102.

25 S. W. Cranford and M. J. Buehler, *CARBON*, 2011, **49**, 4111.

26 Y. M. Lin, C. Dimitrakopoulos, K. A. Jenkins, D. B. Farmer, H. Y. Chiu, A. Grill and P. Avouris, *Science*, 2010, **327**, 662.

27 Y. Ma, Y. Dai, M. Guo and B. Huang, *Phys. Rev. B*, 2012, **85**, 235448.

28 Y. Ma, Y. Dai, M. Guo, C. Niu, Y. Zhu and B. Huang, *ACS Nano*, 2012, **6**, 1695–1701.

29 Y. Ma, Y. Dai, M. Guo, C. Niu, J. Lu and B. Huang, *Phys. Chem. Chem. Phys.*, 2011, **13**, 15546–15553.

30 Y. Ma, Y. Dai, W. Wei, C. Niu, L. Yu and B. Huang, *J. Phys. Chem. C*, 2011, **115**, 20237–20241.

31 Z. H. Aitken and R. Huang, *J. Appl. Phys.*, 2010, **107**, 123531.

32 Q. Peng and S. De, *Physica E*, 2012, **44**, 1662–1666.

33 Q. Peng, A. R. Zamiri, W. Ji and S. De, *Acta Mechanica*, 2012, **707**, 714.

34 Q. Peng, W. Ji and S. De, *Comput. Mater. Sci.*, 2012, **56**, 11.

35 X. Wei, B. Fragneaud, C. A. Marianetti and J. W. Kysar, *Phys. Rev. B*, 2009, **80**, 205407.

36 C. Lee, X. Wei, J. W. Kysar and J. Hone, *Science*, 2008, **321**, 385.

37 M. Crisfield, *Non-Linear Finite Element Analysis of Solids and Structures*, John Wiley & Sons, New York, 1991, p. 18.

38 J. Lubliner, *Plasticity Theory*, Dover Publications, New York, 2008.

39 J. F. Nye, *Physical Properties of Crystals*, Oxford Science Publications, Oxford, 1995.

40 G. Kresse and J. Hafner, *Phys. Rev. B*, 1993, **47**, 558.

41 G. Kresse and J. Hafner, *Phys. Rev. B*, 1994, **49**, 14251.

42 G. Kresse and J. Furthuller, *Phys. Rev. B*, 1996, **54**, 11169.

43 G. Kresse and J. Furthuller, *Comput. Mater. Sci.*, 1996, **6**, 15.

44 P. Hohenberg and W. Kohn, *Phys. Rev.*, 1964, **136**, B864.

45 W. Kohn and L. J. Sham, *Phys. Rev.*, 1965, **140**, A1133.

46 J. Perdew, K. Burke and M. Ernzerhof, *Phys. Rev. Lett.*, 1996, **77**, 3865.

47 P. E. Blöchl, *Phys. Rev. B*, 1994, **50**, 17953–17979.

48 R. O. Jones and O. Gunnarsson, *Rev. Mod. Phys.*, 1989, **61**, 689–746.

49 M. Topsakal, S. Cahangirov and S. Ciraci, *Appl. Phys. Lett.*, 2010, **96**, 091912.

50 Q. Peng, W. Ji and S. De, 2012.

51 F. Everest, *The Master Handbook of Acoustics*, McGraw-Hill, New York, 2001.

52 E. R. Benes, R. Groschl, F. Seifert and A. Pohl, *IEEE Transactions On Ultrasonics Ferroelectrics And Frequency Control*, 1998, **45**, 1314–1330.

53 R. Weigel, D. P. Morgan, J. M. Owens, A. Ballato, K. M. Lakin, K. Hashimoto and C. C. W. Ruppel, *Microwave Theory and Techniques, IEEE Transactions on*, 2002, **50**, 738–749.